J Biol Phys (2015) 41:9–22
DOI 10.1007/s10867-014-9362-z

ORIGINAL PAPER

Prediction of matrix-to-cell stress transfer in heart valve tissues

Siyao Huang · Hsiao-Ying Shadow Huang

Received: 29 May 2014 / Accepted: 12 August 2014 / Published online: 9 October 2014

Abstract Non-linear and anisotropic heart valve leaflet tissue mechanics manifest principally from the stratification, orientation, and inhomogeneity of their collagenous microstructures. Disturbance of the native collagen fiber network has clear consequences for valve and leaflet tissue mechanics and presumably, by virtue of their intimate embedment, on the valvular interstitial cell stress–strain state and concomitant phenotype. In the current study, a set of virtual biaxial stretch experiments were conducted on porcine pulmonary valve leaflet tissue photomicrographs via an image-based finite element approach. Stress distribution evolution during diastolic valve closure was predicted at both the tissue and cellular levels. Orthotropic material properties consistent with distinct stages of diastolic loading were applied. Virtual experiments predicted tissue- and cellular-level stress fields, providing insight into how matrix-to-cell stress transfer may be influenced by the inhomogeneous collagen fiber architecture, tissue anisotropic material properties, and the cellular distribution within the leaflet tissue. To the best of the authors' knowledge, this is the first study reporting on the evolution of stress fields at both the tissue and cellular levels in valvular tissue and thus contributes toward refining our collective understanding of valvular tissue micromechanics while providing a computational tool enabling the further study of valvular cell–matrix interactions.

Keywords Finite element method · Heart valve tissues · Biomechanics · Stress analysis · Collagen fiber orientation · Tissue engineering

1 Introduction

With at least 250,000 patients suffering from heart valve diseases in the United States [1, 2], it is essential that ever more effective heart valve replacements be developed, particularly for pediatric patients, for whom multiple reoperations are often required to account for somatic growth. Building upon knowledge established through nonviable bioprosthetics and cryopreserved valved homografts, tissue engineering of viable replacement heart valves from patients' own cells has been under development since 1995, with the distinction being their unique potential for self-acting tissue repair, growth, and remodeling [3–5]. However, while

S. Huang · H.-Y. S. Huang (✉)
Mechanical and Aerospace Engineering Department, North Carolina State University, R3158 Engineering Building 3, Campus Box 7910, 911 Oval Drive, Raleigh, NC 27695, USA
e-mail: hshuang@ncsu.edu

significant progress has been made and candidate mechanostimulatory factors identified, it remains unclear how best to mechanically condition tissue engineered heart valves (TEHV) and, ultimately, how well TEHVs can mimic native valvular structure and function. Toward addressing these and other unresolved questions concerning valvular structure–function correlates, it is essential to continue refining our understanding of the microstructure and mechanical properties of native heart valves, particularly stress transfer from the extracellular matrix (ECM) to valvular interstitial cells (VICs).

The ECM largely comprises collagens, elastin, and glycosaminoglycans, which in coordination confer valves their mechanical integrity and unique functional characteristics [6–8]. The non-linear and anisotropic mechanical behaviors of aortic and pulmonary valve leaflet tissues have been comprehensively quantified and constitutively modeled via biaxial testing [9–14, 63]. It has been observed that progressive collagen fiber rotation into the principal direction of loading, uncrimping, and transverse compaction collectively enable the tissue to withstand diastolic transvalvular pressure [10–12]. Toward understanding valvular failure mechanisms, previous studies have aimed to determine the stress distributions in heart valve leaflet tissues by finite element analysis and homogenization of the collagen fiber distribution [15–18]. However, these previous linear elastic, isotropic, or non-linear anisotropic tissue-level models have yet to incorporate embedded VICs.

Ex vivo bioreactor cultivation of native valvular tissues [19–22] and the in vitro application of stretch or defined substrate stiffness to VICs [23–25] and VIC-based engineered tissues [26, 27] have collectively demonstrated that the VIC phenotype can be modulated by the mechanical environment [28, 29]. Nevertheless, how heart valve leaflet tissue-level stresses and strains manifest locally at the cellular level remains unclear. Huang et al. demonstrated that VIC nuclei can deform in response to the application of diastolic transvalvular pressures [13]. More recently, Lewinsohn et al. demonstrated that strain transfer through the porcine aortic valve leaflet is anisotropic [30]. While strain transfer upon loading in the leaflet radial direction was linear, cellular strains reached only one-third of the tissue level values when stretched in the circumferential direction. In conjunction with the heterogeneous structure of the valve leaflets, it is expected that micromechanical interactions at the VIC–ECM interface may likewise be heterogeneous, eliciting distinct biological signaling at distinct locations within the leaflet. Nonetheless, neither numerical simulations based on simplified homogeneous finite element models nor models excluding cells can fully describe the micromechanical interactions within the heart valve leaflet tissue.

In order to better understand how external mechanical forces can translate into altered VIC stress states, in the current study we adapt our image-based finite element analysis technique to investigate the stress evolution at both the tissue and cellular levels during diastole [31]. Anisotropic tissue-level finite element models were incorporated, wherein three sets of linearized elastic orthotropic material properties were applied in virtual biaxial experiments to simulate stiffness changes associated with distinct stages of diastolic loading.

2 Materials and methods

2.1 Image-based finite element analysis

The imaged-based finite element analysis (FEA) approach applied herein is capable of simulating physiologic biaxial stretching of valvular tissue matrix and cells from photomicrographs of histological tissue sections. Briefly, open-source Object-Oriented Finite Element (OOF2) software [32, 33], developed by the National Institute of Standards and Technology

(Gaithersburg, MD, USA), was used to read an image and to apply various boundary conditions to the finite element model for the determination of the stress field in the virtual materials system. In order to prescribe distinct material properties to individual tissue constituents, we previously developed a pixel selection extension [31] that dynamically interacts with OOF2. The extension utilizes the hue-saturation-intensity (HSI) color space to distinguish objects within the image; for example, cell nuclei (black), collagenous ECM (pink), and pore space (white) can be prescribed distinct material properties in photomicrographs of hematoxylin and eosin (H&E)-stained heart valve leaflet tissue histological sections (Fig. 1). The extension helped to ensure that all pixels in the images were assigned to their appropriate pixel groups and facilitated material property assignments in the FEA process. The current study aims to present an image-based simulation. Micrographs of histological sections stained by Masson's trichrome, Picrosirius red, or combining with immunohistochemistry for confocal microscopy, as well as fixation for transmission electron microscopy, could also be utilized in these image-based simulations.

To reveal the microstructure of the ECM and VICs for microscopic investigation, panoramic histological photomicrographs were prepared in the image-based FEA program (Fig. 1) [13, 14]. Briefly, porcine pulmonary valve (PV) leaflet samples were fixed in 10% (v/v) neutral buffered formalin, paraffin embedded, sectioned, and stained with H&E and the histological slides were digitized as photomicrographs via an optical microscope [13, 14].

2.2 Assumptions adopted in finite element modeling

Heart valve leaflet tissues are highly collagenous and can be characterized as effectively planar, owing to their relatively small thickness (~400 μm) compared to their orthogonal, lateral dimensions (ca. 3 cm for porcine pulmonary valve leaflets) [34]. Therefore, heart valve tissues are sometimes treated as two-dimensional in computational models [31, 35–39]. Moreover, heart valve tissues are subjected to transvalvular pressure (P) generated during diastole in the negative axial (A) direction, such that the tissues must generate resistant loads (T) or stretches in the circumferential (C) and radial (R) directions to balance out the pressure (Fig. 2). The Young–Laplace equation is applied in the current study to relate the pressure difference to the leaflet tension: $T = \frac{P}{2}r$, where T, P, r are leaflet tension, pressure difference and radius of the sample, respectively. Of note, the leaflet is treated as a very thin surface. To study how the collagen fiber microstructure affects stress fields of the valvular tissue, we utilize equibiaxial stretching on the image-based finite element model to represent the boundary conditions of heart valve tissues during diastole and the appropriate stretching is derived from the leaflet tension T via the Young–Laplace equation, as shown in Fig. 2.

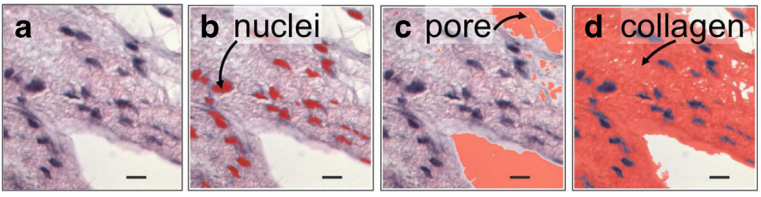

Fig. 1 Illustration of pixel selection extension based on HSI color space. **a** Original histological photomicrograph of a specimen of zero-pressure fixed PV leaflet tissue. **b** Hematoxylin-stained nuclei selected from the original image based on HSI parameters are indicated in *red*. **c** Pore space selected from the original image (*red*). **d** Eosin-stained collagenous ECM selected from the original image (*red*). The extension ensures that all pixels in the images are assigned to their appropriate pixel groups. *Scale bar*=10 μm, x400 original magnification

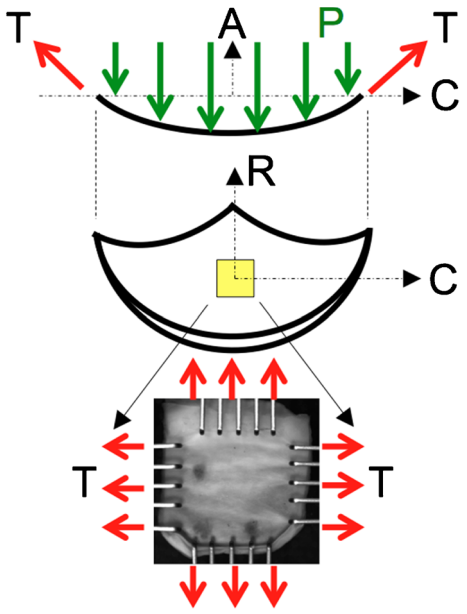

Fig. 2 During diastole, heart valve leaflets are subjected to transvalvular pressure and it is balanced by the tensions T in the C and R directions. The Young–Laplace equation, which demonstrates the relationship between transvalvular pressure difference and leaflet tension, is applied in the current study to relate the pressure difference to the force in the leaflet, where the leaflet is treated as a very thin surface

2.3 Constitutive relations used in finite element simulations

Based on our previous biaxial mechanical analysis of PV leaflet tissue [14], three piecewise linearized elastic orthotropic material property sets associated with distinct toe (0–18%), transition (18–28%), and linear (28–35%) equibiaxial strain ranges (Table 1) were used to obtain the constitutive relation for orthotropic materials capable of simulating non-linear anisotropic material properties within finite element models. Due to the relative thinness of the tissue histological sections imaged (i.e., 4 μm), the finite element model in the current study was considered to be under two-dimensional (2D) plane stress with equibiaxial boundary conditions. For the plane stress material ($\sigma_3=0$, $\tau_{23}=\tau_{13}=0$), the constitutive equation can be reduced to:

$$\begin{Bmatrix} \varepsilon_1 \\ \varepsilon_2 \\ \gamma_{12} \end{Bmatrix} = \begin{bmatrix} S_{11} & S_{12} & 0 \\ S_{21} & S_{22} & 0 \\ 0 & 0 & S_{66} \end{bmatrix} \begin{Bmatrix} \sigma_1 \\ \sigma_2 \\ \sigma_{12} \end{Bmatrix} \text{and } \varepsilon_3 = S_{31}\sigma_1 + S_{32}\sigma_2, \tag{1}$$

where S_{ij} is the compliance matrix ($i, j=1, \ldots, 6$), ε and γ are the strains and σ and τ are the stresses. The 2D compliance matrix for orthotropic materials can be determined via the moduli of elasticity E_i, Poisson's ratios ν_{ij}, and the shear moduli G_{ij} [40, 41]:

$$[S] = \begin{bmatrix} S_{11} & S_{12} & 0 \\ S_{21} & S_{22} & 0 \\ 0 & 0 & S_{66} \end{bmatrix} = \begin{bmatrix} \frac{1}{E_1} & -\frac{\nu_{21}}{E_2} & 0 \\ -\frac{\nu_{12}}{E_1} & \frac{1}{E_2} & 0 \\ 0 & 0 & \frac{1}{G_{12}} \end{bmatrix}, \tag{2}$$

Table 1 Modulus of elasticity of valvular tissues from reference [14]. (a) Modulus of elasticity in zone 1. (b) Tangent modulus of elasticity in zones 2 and 3

E (kPa)	0–18% of strain (zone 1)	
a		
PV X-direction (E_{PVx}^{1})	11.31±0.79	
PV Y-direction (E_{PVy}^{1})	11.67±0.61	
b		
E^{tan} (kPa)	18–28% of strain (zone 2)	28–35% of strain (zone 3)
PV X-direction (E_{PVx}^{tan})	408.23±18.34	1,457.19±58.1
PV Y-direction (E_{PVy}^{tan})	50.16±2.01	172.44±5.24

and consequently the stiffness matrix [C] can be obtained as follows:

$$[C] = [S]^{-1} = \begin{bmatrix} \frac{E_1}{1-\nu_{12}\nu_{21}} & \frac{E_1\nu_{21}}{1-\nu_{12}\nu_{21}} & 0 \\ \frac{E_2\nu_{12}}{1-\nu_{12}\nu_{21}} & \frac{E_2}{1-\nu_{12}\nu_{21}} & 0 \\ 0 & 0 & G_{12} \end{bmatrix} \tag{3}$$

The Poisson's ratio ν_{12} was assumed to be 0.45 for the orthotropic collagen fibers and ν_{21} was derived from the relation $\nu_{21}=\nu_{12}\,E_2/E_1$ [40, 41]. By contrast, cells were considered as isotropic materials (E_{cell}=0.9 kPa and ν_{cell}=0.45) [13, 42]; pore space was an isotropic material as well (E_{pore}=0.01 kPa and ν_{pore}=0.45). The shear moduli were obtained from the relation $G_{ij} = \sqrt{E_iE_j}/\left[2\left(1+\sqrt{\nu_{ij}\nu_{ji}}\right)\right]$, where i, j=1, 2. As a result, the following three stiffness matrices for the porcine PV leaflet tissue were calculated based on data in [14, 43]:

$$[C]_{\text{zone I}} = \begin{bmatrix} 14 & 7 & 0 \\ 7 & 16 & 0 \\ 0 & 0 & 4 \end{bmatrix} (\text{KPa}), \quad [C]_{\text{zone II}} = \begin{bmatrix} 418 & 23 & 0 \\ 23 & 51 & 0 \\ 0 & 0 & 61 \end{bmatrix} (\text{KPa}) \text{ and}$$
$$[C]_{\text{zone III}} = \begin{bmatrix} 1493 & 79 & 0 \\ 79 & 176 & 0 \\ 0 & 0 & 217 \end{bmatrix} (\text{KPa}) \tag{4}$$

2.4 Biomimetic virtual experiments

To predict the tissue-level stress evolution in the PV leaflet tissue during diastolic loading, six sets of virtual experiments were conducted to simulate sub- to supra-physiological biaxial strains. In particular, equibiaxial strains ranging from 10 to 35% were simulated in increments of 5%, with the highest strains (35%) more representative of those incurred by the aortic valve during diastole [13] and thus what might be expected in the PV upon ectopic transplantation, such as in the Ross procedure [6, 8, 44].

In the process of the FEA modeling, the selected histological photomicrograph (1,000× 1,000 pixels) captured the inhomogeneous collagen fiber microstructure and cell nucleus

morphologies (Fig. 3a, b). Pixel groups were selected to represent different materials by color and each group was prescribed distinct material properties. The four-node quadrilateral plane stress element type was applied and the boundary conditions were varied from 10 to 35% equibiaxial stretching at increments of 5% (Fig. 3c). To better visualize the stress distribution within the tissue samples, nine sub-regions were defined (Fig. 3d).

To obtain the stress evolution around a single-cell nucleus, a representative VIC was selected from region 2. Since it was challenging to obtain the location data of the cell in the original photomicrograph (Fig. 3e), the VIC was selected based on the σ_1 contour that evolved under the 35% equibiaxial strain condition (Fig. 3f). To evaluate the stress evolution of said VIC, 21 point locations around the cell boundary were defined (Fig. 3f). Due to the rigid body motion of the cell, it was noted that the contour of the VIC nucleus after stretching was slightly different from the outline of the cell in the original photomicrograph (Fig. 3e).

3 Results

The FEA results illustrated distinct features of the stress distribution in PV leaflet samples under equibiaxial stretching (Fig. 4). Figure 4a–c presents stress fields from the PV model under 15% strain. As expected, based on the higher moduli of elasticity prescribed for the circumferential versus radial directions, the overall circumferential stresses (σ_1) were predicted to be higher than the radial stresses (σ_2) and shear stresses (τ_{12}) in all models. In particular, the differences between σ_1 and σ_2 or τ_{12} were visually evident under the simulated application of 30% equibiaxial strain (Fig. 4d–f). To better understand the changes in stress around the cell

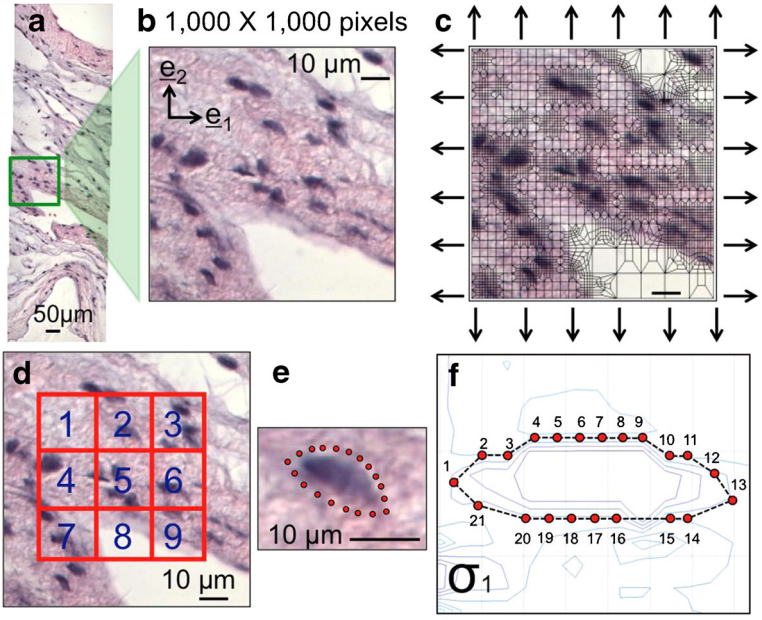

Fig. 3 Virtual experiments on porcine PV leaflet tissue histological photomicrographs. **a** Photomicrograph of an H&E-stained en face PV leaflet tissue section. **b** A 1,000×1,000-pixel region of interest. **c** Application of boundary conditions to the meshed image. **d** Definition of nine sub-regions of interest to facilitate visualization of the stress distributions. **e** Selection of a representative VIC in an unstressed state. **f** Selection of 21 points around the cell nucleus perimeter

nuclei in the PV tissue model during equibiaxial stretching, three locations were selected, as denoted by an arrow (A) with coordinates (182,556), a box (B) with coordinates (460,492) and a circle (C) with coordinates (203,300) in regions 4, 5, and 7, respectively (Fig. 4). Moderate stresses were observed around the perimeters of cell nuclei for tissue models under 15% strain stretching: σ_1 at location A is 1.75 kPa, at location B is 3.79 kPa, and at location C is 3.54 kPa (Fig. 4a), σ_2 at location A is 1.42 kPa, at location B is 2.03 kPa, and at location C is 3.96 kPa (Fig. 4b) and τ_{12} at location A is −0.34 kPa, at location B is 0.57 kPa, and at location C is 1.72 kPa (Fig. 4c). In contrast, much higher stresses were observed for tissue models under 30% strain: σ_1 at location A is 1,292.15 kPa, at location B is 1,139.38 kPa, and at location C is 746.84 kPa (Fig. 4d), σ_2 at location A is 81.72 kPa, at location B is 82.4 kPa and at location C is 185.33 kPa (Fig. 4e), and τ_{12} at location A is −111.48 kPa, at location B is 161.76 kPa, and at location C is 301.01 kPa (Fig. 4f).

For other sets of virtual experiments, the ratio of σ_1 under 35% strain to that under 10% strain was predicted to be 1,288 ($\sigma^{35\%}$ / $\sigma^{10\%}$=1,507.51 kPa/1.17 kPa = 1,288). Interestingly, the ratio of σ_2 under 35% strain to that under 10% strain was predicted to be only 100 ($\sigma^{35\%}$ / $\sigma^{10\%}$=95.35 kPa/0.95 kPa = 100). That is, σ_1 rapidly increased while σ_2 changed relatively modestly between 10 and 35% strain. A similar trend was evident for changes in stress at locations B and C. Localized high stresses around the perimeter of the cell nuclei were thus predicted by the model to be direction-dependent (i.e., anisotropic), suggesting that the preferred collagen fiber direction has a greater effect on how the forces are transmitted to

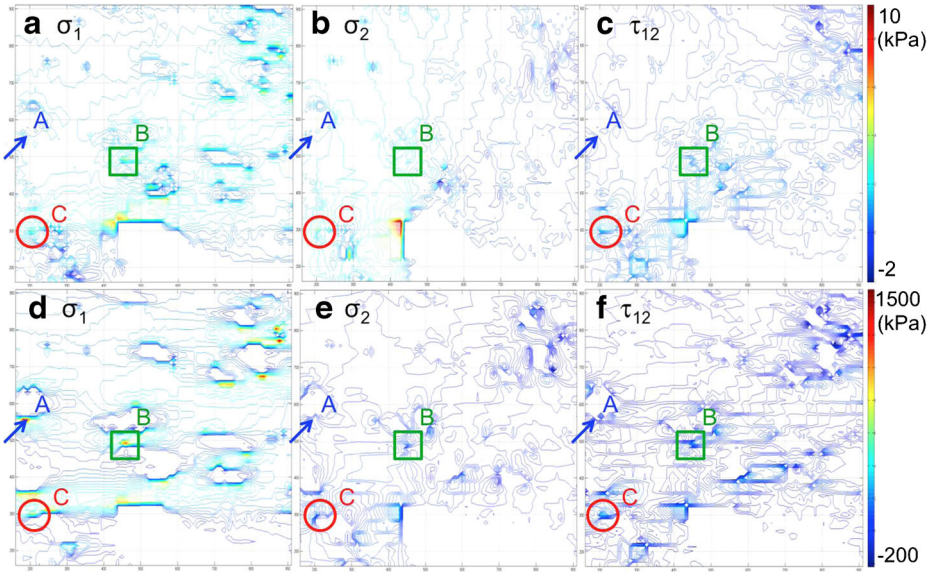

Fig. 4 Stress distribution of the anisotropic finite element model under 15% and 30% equibiaxial strains, respectively. Select locations with coordinates (182,556), (460,492), and (203,300) are denoted by an *arrow* (A), a *box* (B), and a *circle* (C), respectively. High stresses were observed around the perimeters of cell nuclei. **a** σ_1 at location A is 1.75 kPa, at location B is 3.79 kPa, and at location C is 3.54 kPa. **b** σ_2 at location A is 1.42 kPa, at location B is 2.03 kPa, and at location C is 3.96 kPa. **c** τ_{12} at location A is −0.34 kPa, at location B is 0.57 kPa, and at location C is 1.72 kPa. Color key: blue=−2 (kPa) and red=10 (kPa). **d** σ_1 at location A is 1,292.15 kPa, at location B is 1,139.38 kPa, and at location C is 746.84 kPa. **e** σ_2 at location A is 81.72 kPa, at location B is 82.4 kPa, and at location C is 185.33 kPa. **f** τ_{12} at location A is −111.48 kPa, at location B is 161.76 kPa, and at location C is 301.01 kPa. Color key: *blue*=−200 (kPa) and *red*=1,500 (kPa)

cells. Such higher stresses may be transduced by VICs into regulatory signals, as discussed in the next section.

Furthermore, the VIC location also appeared to be an important factor affecting the stresses around the cell nuclei. For example, comparing locations A and B among the six sets of virtual experiments, it was noted that higher σ_1 stresses were predicted at location A. Comparing locations A and C among the six sets of virtual experiments, it was observed that higher σ_2 stresses were predicted at location C. Therefore, it can be speculated that the magnitude of the cellular phenotypic response (e.g., collagen turnover) may be different in the vicinity, for example, of the leaflet free edge or commissures compared to the belly region, owing to the different mechanical stresses associated with each of these structurally and compositionally distinct regions of the valve.

Figure 5 illustrates non-linear stress evolution around the perimeter of a selected VIC. It was observed that σ_1 rapidly increased and reached a maximum at locations 4–9 on the cell nucleus boundary (Fig. 5a). The maximum values of σ_2 were found at locations 1, 2, 3 and 21 on the cell nucleus boundary (Fig. 5b). These results suggest that the magnitude of cellular phenotypic responses may be higher in response to stretching along the boundary parallel to the preferred collagen fiber direction. Corresponding strain evolutions parallel to the circumferential (e_1) and radial (e_2) planes of the representative VIC nucleus are shown in Fig. 5c–d. It is observed that nuclear dimensional changes were greatest in the radial direction, consistent with the larger tissue strains in this direction [7]. The strain evolution along the third direction, i.e., transmural direction, could be calculated based on the incompressibility assumption [45–48] (Fig. 5e). Therefore, a three-dimensional ellipsoidal shape of the VIC nucleus during diastole could then be delineated. Collectively, these simulations predict that the increasing effective load in the circumferential direction due to preferential collagen fiber alignment plays a critical role in determining the high stress that cells experience.

4 Discussion

Decades of experience with valve replacement by nonviable bioprosthetics and cryopreserved allografts has indirectly demonstrated the critical role of VICs in leaflet tissue homeostasis; without the benefit of VIC-mediated ECM maintenance, progressive fatigue-mediated and calcific degeneration are incurred [49]. In pediatric applications, the effective absence of a viable cellular constituent is analogously marked by a lack of normal growth potential [50]. While current valve replacements have been invaluable in the treatment of both acquired and congenital valvular heart disease, the development of improved therapeutic strategies and replacement valves, including TEHVs [9], could benefit from a better understanding of the normal interactions between VICs and their ECM in healthy heart valve leaflets.

Compositionally, morphologically, and mechanically, heart valve leaflet tissues are characterized by their planar and transmural heterogeneity, with the complexity of the distinct free edge, belly, nodulus, and commissure regions [34] compounded perpendicularly by the fibrosa, spongiosa, and ventricularis layers [51]. It is thus reasonable to suspect that all VICs distributed throughout an individual leaflet may not respond identically to physiologic tissue-level stresses and strains: their responses may depend on the local type, concentration and orientation of the collagenous ECM. Indeed, anisotropic and attenuated strain transfer has recently been demonstrated in explanted porcine aortic valve leaflet tissues [30]. Using triads of VIC nuclei as fiducials, local strains calculated at a uniaxially applied tissue-level strain of 30% only reached ~10% and ~20% under circumferential and radial stretches, respectively. Nevertheless, while studies have begun to address the influence of mechanical stretch on

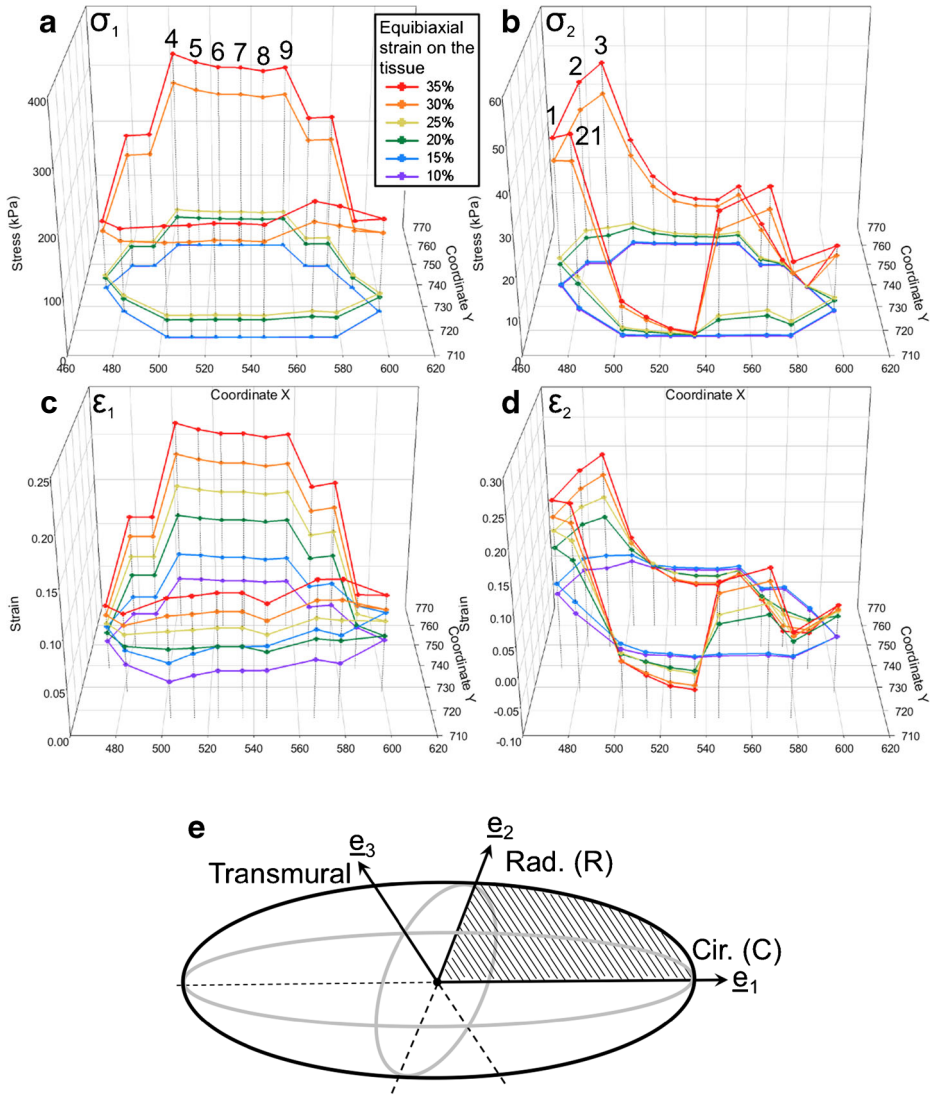

Fig. 5 The stress evolution around a representative VIC nucleus under progressive stretch up to 35% strain. **a** σ_1 at locations 4–9 on the cell boundary rapidly increased and reached a maximum. **b** The highest σ_2 was found at locations 1, 2, 3, and 21. **c**, **d** Corresponding strain evolution of the representative VIC nucleus. **e** The strain evolution along the transmural direction could be calculated based on the incompressibility assumption to obtain a three-dimensional ellipsoidal shape of the VIC nucleus during diastole

in vitro cultured VICs [24, 26, 52–55] and explanted leaflet tissues [19, 20], comparatively few studies have investigated the micromechanical interactions between the VICs and ECM in situ [13, 56], in order to quantify regional stress distributions associated with the heterogeneous ECM or the stress–strain state of an individual VIC.

In the current study, the image-based finite element software OOF2 was used in conjunction with a custom-coded pixel selection extension to predict the stress distribution within heterogeneous porcine PV leaflet tissue, as well as the evolution of stress at the level of an individual

VIC nucleus. Anisotropic tissue-level mechanical properties were incorporated into the finite element model by way of three sets of linearized elastic orthotropic material properties, as derived from our previous biaxial mechanical test results [14]. A limitation of the current study is that the finite element model was solved under small deformation assumptions. Specifically, we provide three sets of linear constitutive relations to describe the mechanical behavior of the valve leaflet; the goal is to describe the non-linear anisotropic material property of tissues as close as possible in our simplified model. When large stretching (above 128%) is applied on the tissue sample, the third set of the linear constitutive equation (Table 1b) could be used to describe the complex material behavior of the tissue. The goal is to provide an easily adopted and simplified method to simulate stress distribution in the heart valve during diastole. As such, an OOF2-based finite element analysis approach implementing finite deformation is currently under development. Another limitation of the current study is that the cell morphologies captured in the photomicrographs and analyzed by the current 2D FE model may not fully recapitulate the 3D morphology and associated changes present in vivo. Moreover, we used a constant material parameter for the cells over the entire range of strains. A refined finite element simulation during diastole is currently being developed considering a varied cell modulus at all stages of strains.

The results of the current study indicate that the stress transmitted from the ECM to the VICs is dependent on the heterogeneous collagen fiber architecture, VIC distribution, and the anisotropic tissue properties (Fig. 4). The stress representative VIC may be influenced by the interactions with neighboring VICs and/or the surrounding ECM and is predicted to vary with the location around the perimeter of the cell nucleus (Fig. 5). Several factors may contribute to the stress distribution that evolves within heart valve leaflet tissues, such as the orientation of collagen fibers, morphologies and/or sizes of the VICs and the local composition and degree of crosslinking of the ECM. Moreover, it is well recognized that valvular tissues [57] and VICs [58] are viscoelastic; the effects of viscoelasticity on stress distribution evolution within leaflet tissue and at the level of individual VICs remain to be ascertained.

At the organ level, comparing the four individual heart valves, Merryman et al. demonstrated in ovine leaflet tissues that transvalvular pressure correlated positively with VIC stiffness and collagen synthesis [59]. Hierarchically, the evidence presented herein for the evolution of a heterogeneous stress distribution due to the heterogeneous and anisotropic ECM within the PV leaflet suggests that perhaps more subtle but functionally important, differences in VIC stiffness and collagen synthesis may be present within the individual leaflets. Such differences may be particularly evident at locations of high stress (Fig. 5). Regional differences in VIC-ECM mechanical interactions may be important not only in normal heart valve function but also in the progression of calcific degeneration or adaptation to ectopic transplantation, such as in the functional adaptation of PV autografts to systemic pressures in the Ross procedure [60]. For example, Fisher et al. demonstrated that calcific nodule formation by in vitro cultured porcine aortic VICs is strain dependent [24]. As such, the stress results predicted in the current study (Fig. 5) may be useful in relating such phenomena from in vitro studies back to the in situ setting.

Ultimately, the mechanotransduction of mechanical forces transmitted from organ-level motions of valve leaflets, through the ECM down to VICs, depends on the number and nature of integrin- and other cell adhesion receptor-mediated attachments between the VICs and their surrounding ECM [61]. As the linkage between the VIC and ECM, transmission of forces through these points of attachment may be critical to physiologic function and pathogenesis. For example, disruption of $\alpha_5\beta_1$ integrin binding between in vitro cultured porcine aortic VICs and fibrin or fibronectin substrates results in up-regulation of osteogenic markers, signaling a calcific response [62]. A unique advantage of the image-based finite element approach utilized

herein is that serial histological sections of tissue can be stained not only for general morphology, as by H&E in the present study but also for specific phenotypic markers by immunohistochemical techniques, thereby offering the opportunity to spatially correlate the finite element predicted stress and strain distributions with cell phenotype. As a result, the image-based finite element approach developed in the current study is well suited for further investigations into VIC–ECM interactions.

5 Conclusions

Through image-based finite element analysis of PV leaflet tissue sections, the current study provides insight into the relationships between heart valve mechanics, microstructure, and material properties. In particular, the virtual experiments conducted herein complement previous studies of VICs and valve mechanics by predicting the stress distribution evolution within the ECM and at the level of an individual VIC. This approach, incorporating the collagen fiber architecture, VIC distributions and the anisotropic material properties of the ECM, provides a tool for comprehensively quantifying the stresses during diastolic valve closure. Through the investigation of VIC–ECM mechanical interactions in healthy heart valve leaflets, results of the current study may be useful in understanding the pathogenesis of valvular diseases and in guiding the development of improved therapeutic approaches and valve replacements.

Acknowledgments The studies presented herein were supported by start-up funds provided by the North Carolina State University Department of Mechanical and Aerospace Engineering.

Competing interests None declared.

Funding The studies presented herein were supported by start-up funds provided by the North Carolina State University Department of Mechanical and Aerospace Engineering.

Ethical approval Not required.

References

1. American Heart Association.: Heart Disease and Stroke Statistics. (2010)
2. NIH. Heart and Vascular Diseases. National Heart Lung and Blood Institute, (2010)
3. El Khoury, G., Vanoverschelde, J.L., Glineur, D., Pierard, F., Verhelst, R.R., Rubay, J., Funken, J.C., Watremez, C., Astarci, P., Lacroix, V., Poncelet, A., Noirhomme, P.: Repair of bicuspid aortic valves in patients with aortic regurgitation. Circulation **114**, I610–I616 (2006)
4. El Oakley, R., Kleine, P., Bach, D.S.: Choice of prosthetic heart valve in today's practice. Circulation **117**(2), 253–256 (2008)
5. Mendelson, K., Schoen, F.J.: Heart valve tissue engineering: Concepts, approaches, progress, and challenges. Ann. Biomed. Eng. **34**(12), 1799–1819 (2006)
6. Christie, G.W., Barratt-Boyes, B.G.: Mechanical properties of porcine pulmonary valve leaflets—how do they differ from aortic leaflets. Ann. Thorac. Surg. **60**(2), S195–S199 (1995)
7. Billiar, K.L., Sacks, M.S.: Biaxial mechanical properties of the natural and glutaraldehyde treated aortic valve cusp - Part I: Experimental results. J. Biomech. Eng.-Trans. ASME **122**(1), 23–30 (2000)

8. Stradins, P., Lacis, R., Ozolanta, I., Purina, B., Ose, V., Feldmane, L., Kasyanov, V.: Comparison of biomechanical and structural properties between human aortic and pulmonary valve. Eur. J. Cardio-thoracic Surg.: Eur. J. Cardio-Thoracic Surg. **26**(3), 634–639 (2004)
9. Sacks, M.S., Schoen, F.J., Mayer, J.E.: Bioengineering challenges for heart valve tissue engineering. Annu. Rev. Biomed. Eng. **11**, 289–313 (2009)
10. Sacks, M.S., Smith, D.B., Hiester, E.D.: The aortic valve microstructure: Effects of transvalvular pressure. J. Biomed. Mater. Res. **41**(1), 131–141 (1998)
11. Joyce, E.M., Liao, J., Schoen, F.J., Mayer Jr., J.E., Sacks, M.S.: Functional collagen fiber architecture of the pulmonary heart valve cusp RID F-3703-2011. Ann. Thorac. Surg. **87**(4), 1240–1249 (2009)
12. Cox, M.A.J., Kortsmit, J., Driessen, N., Bouten, C.V.C., Baaijens, F.P.T.: Tissue-engineered heart valves develop native-like collagen fiber architecture. Tissue Eng. Part a **16**(5), 1527–1537 (2010)
13. Huang, H.-Y.S., Liao, J., Sacks, M.S.: In-situ deformation of the aortic valve interstitial cell nucleus under diastolic loading. J. Biomech. Eng. **129**, 1–10 (2007)
14. Huang, H.-Y.S., Balhouse, B.N., Huang, S.: Application of simple biomechanical and biochemical tests to heart valve leaflets: implications for heart valve characterization and tissue engineering. Proc. Inst. Mech. Eng. H J. Eng. Med. **226**(11), 868–876 (2012)
15. Li, J., Luo, X.Y., Kuang, Z.B.: A nonlinear anisotropic model for porcine aortic heart valves. J. Biomech. **34**(10), 1279–1289 (2001)
16. Luo, X.Y., Li, W.G., Li, J.: Geometrical stress-reducing factors in the anisotropic porcine heart valves. J. Biomech. Eng.-Trans. ASME **125**(5), 735–744 (2003)
17. Mohammadi, H., Bahramian, F., Wan, W.: Advanced modeling strategy for the analysis of heart valve leaflet tissue mechanics using high-order finite element method. Med. Eng. Phys. **31**(9), 1110–1117 (2009)
18. Koch, T.M., Reddy, B.D., Zilla, P., Franz, T.: Aortic valve leaflet mechanical properties facilitate diastolic valve function RID C-3386-2009. Comput. Methods Biomech. Biomed. Eng. **13**(2), 225–234 (2010)
19. Balachandran, K., Konduri, S., Sucosky, P., Jo, H., Yoganathan, A.P.: An ex vivo study of the biological properties of porcine aortic valves in response to circumferential cyclic stretch. Ann. Biomed. Eng. **34**(11), 1655–1665 (2006)
20. Merryman, W.D., Lukoff, H.D., Long, R.A., Engelmayr Jr., G.C., Hopkins, R.A., Sacks, M.S.: Synergistic effects of cyclic tension and transforming growth factor-β1 on the aortic valve myofibroblast. Cardiovasc. Pathol. **16**(5), 268–276 (2007)
21. Metzler, S.A., Digesu, C.S., Howard, J.I., Filip To, S.D., Warnock, J.N.: Live en face imaging of aortic valve leaflets under mechanical stress. Biomech. Model. Mechanobiol. **11**(3–4), 355–361 (2012)
22. Weston, M.W., Yoganathan, A.P.: Biosynthetic activity in heart valve leaflets in response to in vitro flow environments. Ann. Biomed. Eng. **29**(9), 752–763 (2001)
23. Hutcheson, J.D., Venkataraman, R., Baudenbacher, F.J., Merryman, W.D.: Intracellular Ca(2+) accumulation is strain-dependent and correlates with apoptosis in aortic valve fibroblasts. J. Biomech. **45**(5), 888–894 (2012)
24. Fisher, C.I., Chen, J., Merryman, W.D.: Calcific nodule morphogenesis by heart valve interstitial cells is strain dependent. Biomech. Model. Mechanobiol. **12**(1), 5–17 (2013)
25. Quinlan, A.M., Billiar, K.L.: Investigating the role of substrate stiffness in the persistence of valvular interstitial cell activation. J. Biomed. Mater. Res. A **100**(9), 2474–2482 (2012)
26. Gould, R.A., Chin, K., Santisakultarm, T.P., Dropkin, A., Richards, J.M., Schaffer, C.B., Butcher, J.T.: Cyclic strain anisotropy regulates valvular interstitial cell phenotype and tissue remodeling in three-dimensional culture. Acta Biomater. **8**(5), 1710–1719 (2012)
27. Waxman, A.S., Kornreich, B.G., Gould, R.A., Moise, N.S., Butcher, J.T.: Interactions between TGFβ1 and cyclic strain in modulation of myofibroblastic differentiation of canine mitral valve interstitial cells in 3D culture. J. Vet. Cardiol. **14**(1), 211–221 (2012)
28. Eastwood, M., McGrouther, D.A., Brown, R.A.: Fibroblast responses to mechanical forces. Proc. Inst. Mech. Eng. Part H-J. Eng. Med. **212**(H2), 85–92 (1998)
29. Liu, W.F. Mechanical regulation of cellular phenotype: implications for vascular tissue regeneration. Cardiovasc. Res. **95**(2), 215–222 (2012)
30. Lewinsohn, A.D., Anssari-Benham, A., Lee, D.A., Taylor, P.M., Chester, A.H., Yacoub, M.H., Screen, H.R.C.: Anisotropic strain transfer through the aortic valve and its relevance to the cellular mechanical environment. Proc. Inst. Mech. Eng. Part H-J. Eng. Med. **225**(H8), 821–830 (2011)
31. Huang, S., Huang, H.-Y.S.: Virtualisation of stress distribution in heart valve tissue. Comput. Methods Biomech. Biomed. Eng. **17**(15), 1696–1704 (2014). doi:10.1080/10255842.2013.763937
32. Langer, S.A., Fuller, E., Carter, W.C.: OOF: An image-based finite-element analysis of material microstructures. Comput. Sci. Eng. **3**(3), 15–23 (2001)
33. Reid, A.C.E., Lua, R.C., Garcia, R.E., Coffman, V.R., Langer, S.A.: Modelling microstructures with OOF2. Int. J. Mater. Prod. Tech. **35**(3–4), 361–373 (2009)

34. Mirnajafi, A., Raymer, J.M., McClure, L.R., Sacks, M.S.: The flexural rigidity of the aortic valve leaflet in the commissural region. J. Biomech. **39**(16), 2966–2973 (2006)
35. Sun, W., Huang, H.-Y.S., Argento, M.S. and Sacks, M.S. Finite element implementation of a structural constitutive model for planar collagenous tissues. 2003 Proceedings of the Second MIT Conference on Computational Solid and Fluid Mechanics, Cambridge, MA, (2003)
36. Sun, W., Sacks, M.S.: Finite element implementation of a generalized Fung-elastic constitutive model for planar soft tissues. Biomech. Model. Mechanobiol. **4**(2–3), 190–199 (2005)
37. Sun, W., Sacks, M.S., Sellaro, T.L., Slaughter, W.S., Scott, M.J.: Biaxial mechanical response of bioprosthetic heart valve biomaterials to high in-plane shear. J. Biomech. Eng. **125**(3), 372–380 (2003)
38. Huang, S. and Huang, H.-Y.S. Virtual Experiments of Heart Valve Tissue. IEEE Engineering in Medicine and Biology Society, pp. 6645–6648 (IEEE, San Diego, CA, 2012).
39. Huang, S. and Huang, H.-Y.S. Tissue- and cell-levels stress distribution of heart valve tissue during diastole. Proceedings of the ASME International Mechanical Engineering Congress and Exposition, (2013).
40. Nye, J.F. Physical properties of crystals, their representation by tensors and matrices. Oxford, Clarendon Press (1957).
41. Slaughter, W.S.: The Linearized Theory of Elasticity. Birkhauser, Boston (2001)
42. Zhao, R.G., Wyss, K., Simmons, C.A.: Comparison of analytical and inverse finite element approaches to estimate cell viscoelastic properties by micropipette aspiration. J. Biomech. **42**(16), 2768–2773 (2009)
43. Huang, H.-Y.S., Balhouse, B.N. and Huang, S. A Synergy Study of Heart Valve Tissue Mechanics, Microstructures, and Collagen Concentration. 2012 ASME International Mechanical Engineering Congress and Exposition ASME, Houston (2012)
44. David, H., Boughner, D.R., Vesely, I., Gerosa, G.: The pulmonary valve. Is it mechanically suitable for use as an aortic valve replacement? ASAIO J. **40**(2), 206–212 (1994)
45. Lanir, Y.: A structural theory for the homogeneous biaxial stress–strain relationships in flat collagenous tissues. J. Biomech. **12**(6), 423–436 (1979)
46. Lanir, Y.: Constitutive equations for fibrous connective tissues. J. Biomech. **16**(1), 1–12 (1983)
47. Lanir, Y.: A microstructure model for the rheology of mammalian tendon. ASME Journal of Biomechanical Engineering, **102**(4), 332–339 (1980)
48. Lanir, Y.: Plausibility of structural constitutive equations for isotropic soft tissue in finite static deformations. J. Appl. Mech. **61**, 695–702 (1994)
49. Sacks, M.S., Schoen, F.J.: Collagen fiber disruption occurs independent of calcification in clinically explanted bioprosthetic heart valves. J. Biomed. Mater. Res. **62**(3), 359–371 (2002)
50. Perron, J., Moran, A.M., Gauvreau, K., del Nido, P.J., Mayer, J.E., Jonas, R.A.: Valved homograft conduit repair of the right heart in early infancy. Ann. Thorac. Surg. **68**(2), 542–548 (1999)
51. Stella, J.A., Sacks, M.S.: On the biaxial mechanical properties of the layers of the aortic valve leaflet. J. Biomech. Eng.-Trans. ASME **129**(5), 757–766 (2007)
52. Gupta, V., Tseng, H., Lawrence, B.D., Grande-Allen, K.J.: Effect of cyclic mechanical strain on glycosaminoglycan and proteoglycan synthesis by heart valve cells. Acta Biomater. **5**(2), 531–540 (2009)
53. Ku, C.-H., Johnson, P.H., Batten, P., Sarathchandra, P., Chambers, R.C., Taylor, P.M., Yacoub, M.H., Chester, A.H.: Collagen synthesis by mesenchymal stem cells and aortic valve interstitial cells in response to mechanical stretch. Cardiovasc. Res. **71**(3), 548–556 (2006)
54. Smith, K.E., Metzler, S.A., Warnock, J.N.: Cyclic strain inhibits acute pro-inflammatory gene expression in aortic valve interstitial cells. Biomech. Model. Mechanobiol. **9**(1), 117–125 (2010)
55. Throm Quinlan, A.M., Sierad, L.N., Capulli, A.K., Firstenberg, L.E., Billiar, K.L.: Combining dynamic stretch and tunable stiffness to probe cell mechanobiology in vitro. PLoS ONE **6**(8), e23272 (2011)
56. Carruthers, C.A., Alfieri, C.M., Joyce, E.M., Watkins, S.C., Yutzey, K.E., Sacks, M.S.: Gene expression and collagen fiber micromechanical interactions of the semilunar heart valve interstitial cell. Cell. Mol. Bioeng. **5**(3), 254–265 (2012)
57. Stella, J.A., Liao, J., Sacks, M.S.: Time-dependent biaxial mechanical behavior of the aortic heart valve leaflet. J. Biomech. **40**(14), 3169–3177 (2007)
58. Merryman, W.D., Bieniek, P.D., Guilak, F. and Sacks, M.S. Viscoelastic Properties of the Aortic Valve Interstitial Cell. J. Biomech. Eng. **131**(4), 041005 (2009)
59. Merryman, W.D., Youn, I., Lukoff, H.D., Krueger, P.M., Guilak, F., Hopkins, R.A., Sacks, M.S.: Correlation between heart valve interstitial cell stiffness and transvalvular pressure: implications for collagen biosynthesis. Am. J. Physiol.-Heart Circ. Physiol. **290**(1), H224–H231 (2006)
60. Rabkin-Aikawa, E., Aikawa, M., Farber, M., Kratz, J.R., Garcia-Cardena, G., Kouchoukos, N.T., Mitchell, M.B., Jonas, R.A., Schoen, F.J.: Clinical pulmonary autograft valves: pathologic evidence of adaptive remodeling in the aortic site. J. Thorac. Cardiovasc. Surg. **128**(4), 552–561 (2004)
61. Latif, N., Sarathchandra, R., Taylor, R.M., Antoniw, J., Yacoub, M.H.: Molecules mediating cell-ECM and cell-cell communication in human heart valves. Cell Biochem. Biophys. **43**(2), 275–287 (2005)

62. Gu, X., Masters, K.S.: Regulation of valvular interstitial cell calcification by adhesive peptide sequences. J. Biomed. Mater. Res. A **93**(4), 1620–1630 (2010)
63. Huang, H.-Y.S., Huang, S., Frazier, Colin P., Prim, Peter, and Harrysson, O., Directional Mechanical Property of Porcine Skin Tissues. J. Mech. Med. Biol. **14**(5), (2014). doi: 10.1142/S0219519414500699.